Hindawi
Mathematical Problems in Engineering
Volume 2018, Article ID 3245498, 8 pages
https://doi.org/10.1155/2018/3245498

Research Article

Mathematical Model for the Fluid-Gas Spontaneous Displacement in Nanoscale Porous Media considering the Slippage and Temperature

Kang Liu,[1] Zhongyue Lin ,[2,3] Daiyong Cao,[1] and Yingchun Wei[1]

[1]*College of Geoscience and Surveying Engineering, China University of Mining & Technology, Beijing 100083, China*
[2]*Beijing Dadi Gaoke Coalbed Methane Engineering Technology Research Institute, Beijing 100040, China*
[3]*National Administration of Coal Geology in China, Beijing 100038, China*

Correspondence should be addressed to Zhongyue Lin; 53674914@qq.com

Received 25 September 2017; Revised 10 January 2018; Accepted 23 January 2018; Published 15 February 2018

Academic Editor: Sandro Longo

The fracturing fluid-gas spontaneous displacement during the fracturing process is important to investigate the shale gas production and formation damage. Temperature and slippage are the major mechanisms underlying fluid transport in the micro-/nanomatrix in shale, as reported in the previous studies. We built a fracturing fluid-gas spontaneous displacement model for the porous media with micro-/nanopores, considering two major mechanisms. Then, our spontaneous displacement model was verified by the experimental result of the typical shale samples and fracturing fluids. Finally, the influences of temperature, slip length, and pore size distribution on the spontaneous imbibition process were discussed. Slippage and temperature significantly influenced the imbibition process. Lower viscosity, higher temperature, and longer slip length increased the imbibition speed. Ignoring the temperature change and slippage will lead to significant underestimation of the imbibition process.

1. Introduction

During hydraulic fracturing process in the unconventional gas formation, a relatively large volume of fracturing fluid is pumped into formation, which can greatly stimulate the gas production [1, 2]. In this process, water will be imbibed into matrix in the fractured reservoir by many influences, including capillary pressure [3–5], chemical osmotic pressure [6], pore network [7–9], and clay mineral [10], which is called spontaneous imbibition. Also, leakage, lost circulation, and induced fracture in drilling process will lead to fracturing fluid being pumped into formation [11–13], which will also cause imbibition process and may change the stress field near wellbore [14] and drilling state [15, 16]. The spontaneous imbibition is the dominant mechanism of the water transport into the formation because of the high capillary pressure by nanopores [17–19]. Recently studies have shown that the spontaneous imbibition of fracturing fluid can be a driving force to enhance the gas recovery for shale gas reservoir [20, 21]. Thus, analysis of the spontaneous imbibition of shale and the potential effect on gas recovery needs urgent attention.

Shale has an ultralow permeability and porosity with abundant nanopores. Liquid flow mechanism in shale is much more complex than conventional formations. Slip flow is a major mechanism of liquid transport in nanotube [22, 23]. More studies have shown that the slip flow is significantly different from the no-slip boundary condition in the nanotubes [24, 25]. In addition, these studies reported that conventional flow equations, such as Darcy's law, may not be valid for shale systems because of the difference in the controlling physics of liquid flow.

Fracturing fluid commonly includes hydrochloric acid, friction reducers, guar gum, and biocides. Viscosity varies with temperature significantly [26]. Reservoir temperature is also one of the key controlling factors in spontaneous imbibition. The influence of temperature on gas production is usually ignored because the temperature change is not

severe. However, for spontaneous imbibition in the hydraulic fracturing process, the temperature of fracturing liquid is quite different from formation. Thus, ignoring the variation in temperature will lead to inaccurate results and errors.

2. Mathematical Model

2.1. Spontaneous Imbibition considering Slip Effect in a Single Capillary. Spontaneous imbibition occurs in the capillaries of shale as the wetting fluid imbibed in capillaries is driven by capillary force automatically. Liquid slip in nanoscale capillaries is especially not negligible because the slip length is the same scale with the diameter. In this section, considering liquid slip effect, we established a spontaneous imbibition model. To focus on the effect of liquid slip, we have made some simplifications as follows: (1) the cross section of tube is circular; (2) liquid is the wetting phase, while gas is the nonwetting phase; (3) liquid is the Newton liquid with laminar flow, and inertial forces have been ignored; (4) the driving force of spontaneous imbibition is the capillary force; (5) slip occurs at tube wall; and (6) gravity is ignored. On the basis of the Hagen–Poiseuille equation, the fluid flux considering the liquid slip can be calculated as follows:

$$Q = \frac{\pi \Delta p}{32 \mu L_f} \left[\frac{1}{2} \left(\lambda + 2L_s \right)^2 \lambda^2 - \frac{1}{4} \lambda^4 \right], \tag{1}$$

where Q is the fluid flux in tube, Δp is the pressure difference on fluid, μ is the dynamic viscosity, L_f refers to the length of fluid path line, λ is the tube's equivalent diameter, and L_s is the slip length. L_s can be expressed in a dimensionless form, $L_{sD} = L_s/\lambda$.

Imbibition velocity can be determined as follows:

$$v_f = \frac{4Q}{\pi \lambda^2} = \frac{dL_f}{dt}. \tag{2}$$

The real capillary in shale is tortuous. Tortuous fractal dimension is introduced to express the tortuous capillaries, according to Yu and Cheng [27] and Cai et al. [28].

$$\begin{aligned} L_f &= \lambda^{1-D_T} L_0^{D_T}, \\ v_f &= \frac{dL_f}{dt} = D_T \lambda^{1-D_T} L_0^{D_T - 1} v_0, \end{aligned} \tag{3}$$

where L_0 is the distance between meniscus and liquid intake and D_T refers to the fractal dimension of a tortuous capillary.

If (1)–(3) are rearranged, we have the following equation:

$$v_0 = \frac{dL_0}{dt} = \frac{\left[\left(\lambda + 2L_s \right)^2 / 2 - \lambda^2 / 4 \right]}{8 \mu D_T \lambda^{2-2D_T} L_0^{2D_T - 1}} \Delta p. \tag{4}$$

The driving pressure of spontaneous imbibition is the capillary force. Thus, we have the following equation:

$$\Delta p = p_{\text{out}} - p_{\text{in}} = p_c = \frac{4\sigma \cos\theta}{\lambda}, \tag{5}$$

where θ is the contact angle between liquid and tube wall and σ is the interfacial tension. During the imbibition process, the imbibition length is increasing with the movement of meniscus. For the tortuous tube, using the initial condition $L_0|_{t=0} = 0$, the relationship between imbibition length and time can be derived as follows:

$$L_0 = \left\{ \frac{\left[\left(\lambda + 2L_s \right)^2 / 2 - \lambda^2 / 4 \right]}{4 \mu \lambda^{2-2D_T}} \left(\frac{4\sigma \cos\theta}{\lambda} \right) \right\}^{1/2D_T} t^{1/2D_T}. \tag{6}$$

2.2. Pore Size Distribution. Pore size distribution is also important. According to the statistical data by Diamond and Dolch [29] and Hwang and Powers [30], the pore size distribution of the porous media can be simulated by lognormal distribution function. This function is a good way to represent the pore size distribution of the porous media. Thus, the pore space is the generalized lognormal distribution, as follows [29]:

$$f(r) = \frac{1}{\sqrt{2\pi} \ln \sigma_0} \exp \left[- \left(\frac{\ln \left(\lambda' / \overline{\lambda}' \right)}{\sqrt{2} \ln \sigma_0} \right)^2 \right], \tag{7}$$

where $\lambda' = (\lambda - \lambda_{\min})(\lambda_{\max} - \lambda_{\min})/(\lambda_{\max} - \lambda)$, λ is the equivalent diameter of pores, σ_0 and $\overline{\lambda}'$ are the distribution parameters characterizing the distribution properties of λ', $\overline{\lambda}'$ is the mean or expectation of the distribution, and sigma σ_0 is the standard deviation. $f(\lambda)$ is the percent volume of voids in diameter λ. The cumulative distribution function can be expressed as follows:

$$\begin{aligned} F(r) = {} & \frac{1}{\sqrt{2\pi} \ln \sigma_0} \\ & \cdot \int_{\lambda/2}^{\lambda_{\max}/2} \exp \left[- \left(\frac{\ln \left(\lambda' (x) / 2 \right) - \ln \left(\left(\overline{\lambda}' \right) / 2 \right)}{\sqrt{2} \ln \sigma_0} \right)^2 \right] \\ & \cdot \frac{(\lambda_{\max} - \lambda_{\min})}{(\lambda_{\max} - x)(x - \lambda_{\min})} dx, \end{aligned} \tag{8}$$

where $F(\lambda)$ is the percent volume of voids in the diameters larger than λ. According to Diamond and Dolch [29], as σ_0 decreases, pores are more concentrated on the mean or expectation of the distribution $\overline{\lambda}'$; in addition, the peak of the curve is higher. For the capillary bundle model used in this work, the imbibition volume V can be expressed as follows:

$$V = \sum_{\lambda=\lambda_{\min}}^{\lambda_{\max}} f(\lambda) A_r L_f(\lambda), \tag{9}$$

where A_r is the area of cross section.

2.3. Temperature Influences. Viscosity of the fracturing fluid varies with temperature. Normally, viscosity decreases with the increase in the temperature. For simplicity, many empirical or semiempirical equations (correlations) are proposed

Table 1: Basic property of the samples.

Sample	Mass (g)	Diameter (mm)	Length (mm)	Porosity (%)	Dry sample permeability (10^{-6} μm^2)
S1	16.13	25	15	3.49	3.1
S2	15.93	25	15	3.37	2.2
S3	16.34	25	15	4.22	1.9

to describe the temperature dependence of the fluid viscosity [31–33]. According to the observations on the experimental data, $\ln \mu$ is a linear function of the reciprocal absolute temperature $1/T$ in the low temperature range. For the typical fracturing fluid, the relationship between viscosity and temperature follows the Arrhenius equation [31–33]:

$$\mu = A_s \exp \frac{E_a}{RT}, \tag{10}$$

where E_a is the activation energy (Arrhenius energy) of the viscous flow, T is the temperature of liquid, and μ is the apparent viscosity, as is the preexponential factor, and R is the universal gas constant. The constants can be derived by experiment. Equation (10) can be rewritten as follows:

$$\ln \mu = A + \frac{B}{T}, \tag{11}$$

where $A = \ln A_s$ and $B = T^* = E_a/R$ are the Arrhenius activation temperature [33]. Taking (3), (6), (7), and (10) into (9), the spontaneous imbibition model considering the reservoir temperature and slippage effect can be derived.

3. Experiment and Validation

We used three samples from the Longmaxi Marine Shale Formation of Lower Silurian in Sichuan Basin to validate our imbibition model. The basic properties of the samples are shown in Table 1. Sample permeabilities are tested by pulse-decay method on an ultralow permeability measurement instrument. Related introductions have been attached in Appendix. Permeability results are listed in Table 1.

In addition, the core imbibition characteristics are tested in the spontaneous imbibition experiment. This experiment can record the relationship between imbibition volume and imbibition time. We used cocurrent imbibition this time, which can eliminate the influence of mineral dissolution from samples to the imbibed water. The experiments were performed at room pressure (0.1 MPa) and temperature (298 K). Detailed introductions are listed in Appendix.

Mercury intrusion experiment was conducted to measure the pore size distribution. Because mercury intrusion has irreversible negative effect on samples, the mercury intrusion should be arranged after permeability tests and imbibition tests. The schematic diagram of mercury intrusion experiment and detailed procedure of experiment are listed in Appendix.

During the mercury intrusion experiment, as pressure increases, liquid mercury is first injected in the largest pores and was gradually submerged to smaller pores. After the calculation of the mercury injection curve, the results of the pore size distribution for S1, S2, and S3 are shown in Figure 1. In our model, by adjusting the parameters in (8), the pore size distribution for each core sample can be rebuilt when the simulated cumulative distributions follow the experiment curves. Simulated cumulative distributions are also shown in Figure 1.

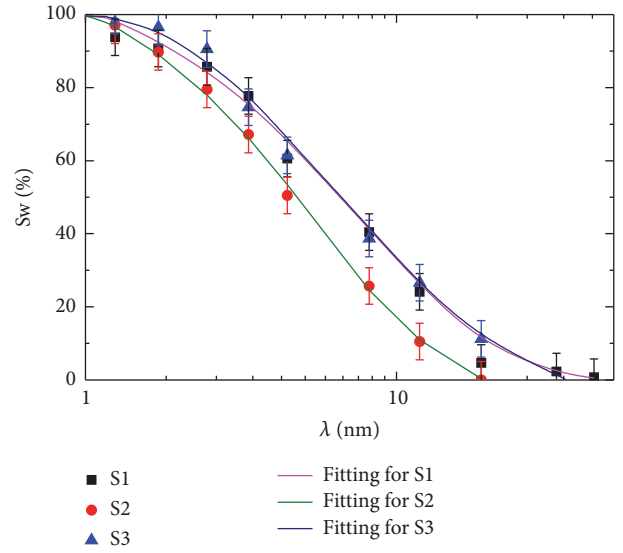

Figure 1: The simulating process for cumulative distributions (S1, S2, and S3).

To derive the rheological parameters, we used an electronic rheometer (NDJ-5K) to test the viscosity-temperature curve. The schematic of instrument is shown in Appendix. The ingredients are shown in Table 2. Their viscosity-temperature relationship data are rearranged in $\ln \mu \sim 1/T$ form to calculate the parameters in the Arrhenius equation. The linear relationship is evident, and the parameters A and B can easily be derived in Figure 2. The results from linear fitting (see (10) and (11)) are shown in Table 2. Fluid viscosity μ reflects the ability of resistance of fluid to gradual deformation by shear stress or tensile stress. Based on the theory of Arrhenius equation, E_a is the activation energy, which reflects the intrinsic property for a liquid. E_a not only indicates the resistant of flow but also indicates the sensibility of temperature for a liquid. We can derive that L2 has higher activation energy, which means the average molecule chain of L2 is rigid or polar. During imbibition process, L2 may not easy to be imbibed in samples. The imbibition result from Figure 4 will give further explanation. Also, according to Haj-Kacem et al. [33], A_s can be closely related to the viscosity of the pure system in vapor state at the same studied pressure [34–37]. From the results of experiment, As_1 and As_2 can be derived, so As_1 and As_2 are approximately the viscosity of L1 and L2 systems at vapor state under the working pressure, if any some molecules pass in vapor state and mix with the gas fluid.

To examine the validation of this model, we draw the spontaneous imbibition curves from the experimental and simulated results for the 3 samples under the same coordinates (Figure 3). The environment parameters in the model

Table 2: Ingredients of the fracturing fluid we used: A is intercept in equation (11); B is Arrhenius activation temperature in equation (11); A_s can be closely related to the viscosity of the pure system in vapor state at the same studied pressure; E_s is the activation energy.

Fracturing fluid	Ingredients	A	B	A_s (mPa·s)	E_s (kl·mol^{-1})
L1	Slick water 100%	0.68	890	1.98	7.40
L2	Slick water 90% + guar gum 10%	−0.31	1553	0.73	12.91

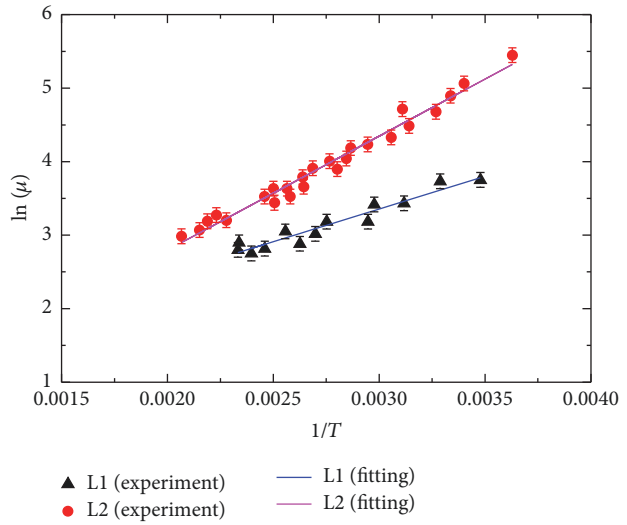

Figure 2: Experimental data for the relationship between viscosity and temperature for L1 and L2.

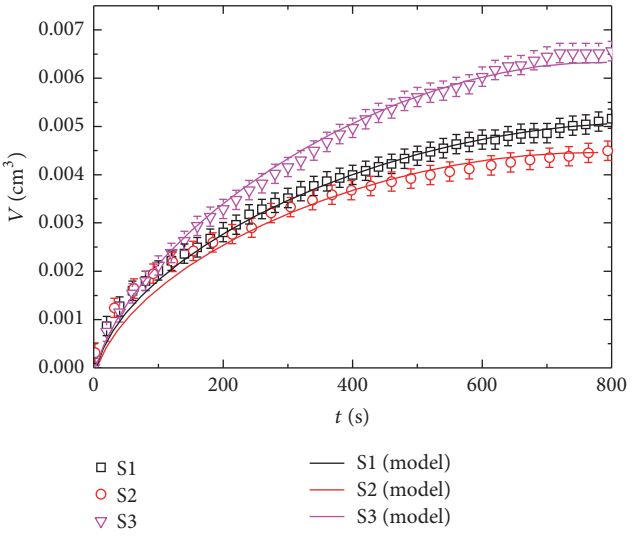

Figure 3: Model verification process for the spontaneous imbibition experimental results and simulated results.

were set the same as those in the experiments. Slick water was used as the imbibition fluid. Under the same working conditions, the result shows that our model coordinates well with the experimental data. Thus, the imbibition function considering slippage was verified. Moreover, the length of our samples is small, and influence of gravity on our model can be neglected. Thus, our model does not include a gravity item.

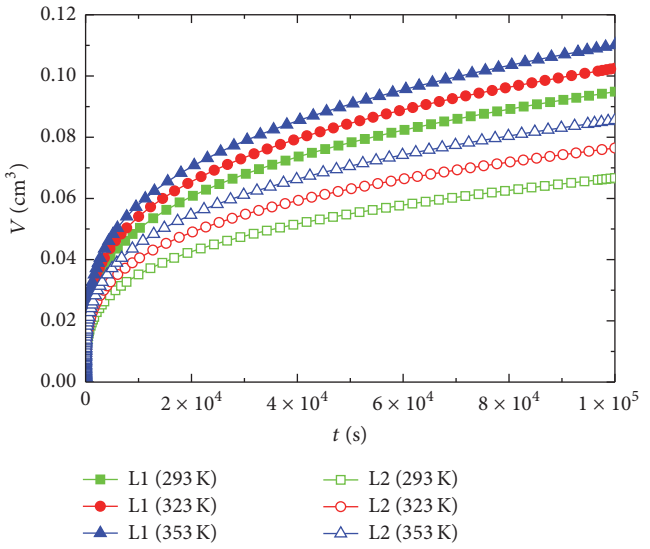

Figure 4: Relationship between imbibition volume and imbibition time at different temperatures for two kinds of fracturing fluids.

4. Results and Discussion

4.1. Temperature. On the basis of the derived spontaneous imbibition model, the effects of temperature, slip length, and pore size distribution have significant influence on the imbibition process. When temperature variation is considered, the rheological parameters of the fracturing fluid vary with the temperature. The imbibition curves for the porous media with the same pore size distribution have been calculated at 3 different temperatures, namely, 20, 50, and 80°C (or 293 K, 323 K, and 353 K), with the nondimensional slip length at 0.1 for two kinds of fracturing fluids (L1 and L2). Figure 4 shows the imbibition curve variation at different temperatures. With the same initial condition, the imbibition volume is 0 at $t = 0$. As temperature increases, the imbibition volume also increases. Under the same temperature, fracturing fluid L2 has higher viscosity than L1; however, its imbibition volume is lower. On the other hand, for the same fracturing fluid, the imbibition volume increases with the increase in temperature. This phenomenon is caused by the following: in environments with lower temperature, fracturing fluid viscosity is higher, making fracturing fluid harder to be imbibed. L2 contains guar gum; thus, its viscosity is higher than that of L1 at the same temperature, which also makes the fracturing fluid harder to be imbibed.

4.2. Slip Length. Considering the scale of micro-/nanopores and silts, the slip effect has a significant influence on the spontaneous imbibition process. The relationship curves of

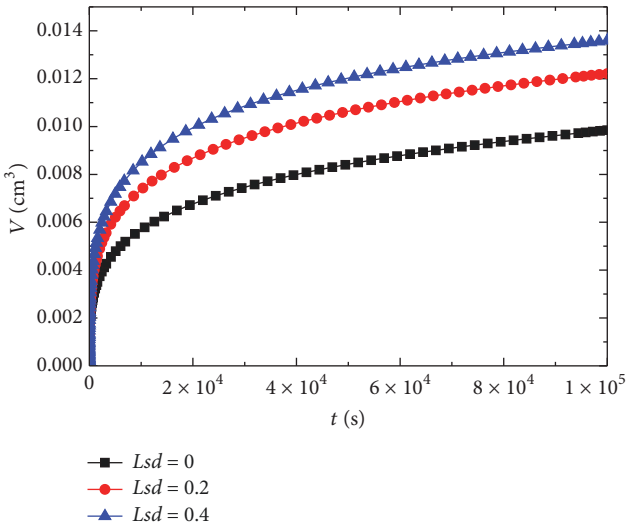

FIGURE 5: Relationship between imbibition volume and imbibition time at different slip lengths.

the imbibition volume and imbibition time under different dimensionless slip length are shown in Figure 5. In this figure, when the temperature is certain, the imbibition volume is gradually increased with increasing dimensionless slip length. Slip effect is much evident in micro-/nanopores in shale. When the dimensionless slip length reaches 0.4, which is about half of the diameter, the imbibition volume increases up to about 30% at the same time compared with the no-slip boundary. Also, as dimensionless slip length increases, the influence on spontaneous imbibition will decrease. Because as dimensionless slip length increases from 0 to 0.2, imbibition volume at $t = 10^5$ increases from 0.009 to 0.012 (with increment 0.003). While dimensionless slip length increases from 0.2 to 0.4, the increment is 0.0015 (from 0.012 to 0.0135).

Slip length mainly exists in the nanoscale pores and silts [22]. In the imbibition analysis for shale, imbibed pore spaces are mainly in the nanoscale, which has the same scale with slip length. Thus, slip length can easily reach 0.4 or higher. Ignorance of the slip effect will lead to significant underestimation of the imbibition speed and volume. When analyzing the spontaneous imbibition process, overlooking slippage will considerably underestimate the imbibition flux, which is special compared with sandstones.

4.3. Pore Size Distribution. Pore size also has significant effects on the imbibition characteristics. The distribution effect can be derived by adjusting the pore size distribution parameters in the spontaneous imbibition model. A total of 3 different kinds of distributions have been discussed, as shown in Figure 6(a). Cases 1 and 2 share the same range of diameter with different peaks, so the mean or expectation of the distributions $\overline{\lambda}'$ is the same, while the standard deviation σ_0 for Case 1 is smaller than that for Case 2. By comparing Cases 1 and 2, the influence of the concentration for pore size on spontaneous imbibition can be analyzed. On the other hand, Cases 2 and 3 share the same peak height with different average diameters, but different average diameter. To analyze the influence of porosity on spontaneous imbibition, the standard deviations σ_0 for Cases 2 and 3 are the same, while the mean or expectation of the distributions $\overline{\lambda}'$ is different. By comparing Cases 2 and 3, we can derive the influence of average pore size on spontaneous imbibition. The simulated imbibition curves are shown in Figure 6(b). Comparing Cases 2 and 3, for the cases with smaller average pores, the imbibition speed is smaller too. From (1), we can derive that flowing flux is proportional to diameter's biquadrate. Smaller pores will gain much more flowing resistance. Meanwhile, for sample with higher peak frequency, the imbibition speed is higher, which means pore space with more concentrate pore size distribution will gain higher imbibition volume.

5. Conclusions

(1) Temperature has influence on the fluid viscosity. Thus, the spontaneous imbibition process can be influenced by temperature. When the slip length is kept stable, the imbibition volume increases with the rise in the temperature at the same imbibition time. Meanwhile, when the temperature is kept unchanged, the imbibition volume increases with the rise in the slip length at the same imbibition time. Additionally, the imbibition rate decreases as imbibition time increases.

(2) Pore size also has significant effects on the imbibition process. With the same peak height of pore size distribution, the imbibition volume decreases with the decline in the average pores at the same imbibition time. On the other hand, with the same average pore diameter, higher peak of pore size distribution than that of the others will gain larger imbibition volume at the same imbibition time.

(3) Temperature and slippage are not negligible in the study of the fracturing fluid-gas spontaneous displacement in shale. Ignoring these two parameters will lead to significant underestimation on the imbibition speed and volume.

Appendix

We have used a series of experiments in this work. Detailed structures and procedures are listed in this Appendix.

The procedures of permeability test are as follows: (a) all samples are dried at temperature 338 K for 12 h before the experiment until the mass remained unchanged. (b) Sample permeability are tested by pulse-decay method on an ultralow permeability measurement instrument (Figure 7). The dried cores are placed in core chamber with confining pressure 5 MPa. The environment is set at 298 K and pore pressure is 2 MPa. Helium is used for sample tests. (c) Repeating the preceding steps 3 times, average permeability for each sample was derived.

In spontaneous imbibition experiment, the sample contacts the liquid at surface. The schematic is presented in Figure 8. The imbibed water volume was measured on line by a balance (METTLER LE204E) connected to a computer, with accuracy of 0.0001 g. The method to obtain the imbibed water volume is shown in Figure 8. The procedures of imbibition test are as follows.

(a) Keep the experimental environment stable at 0.1 MPa and 298 K. The fluctuation of temperature is controlled within

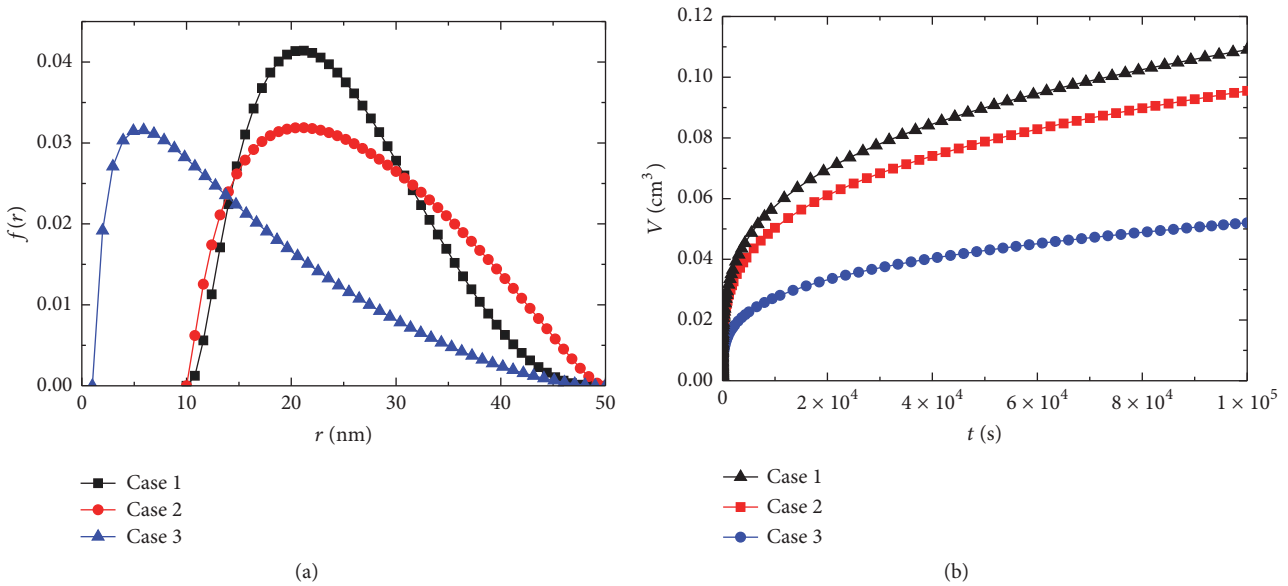

FIGURE 6: Relationship between imbibition volume and imbibition time in different pore size distribution: (a) different kinds of distributions for three cases; (b) simulated imbibition curves for three cases.

FIGURE 7: The photo of the pulse-decay permeability instrument.

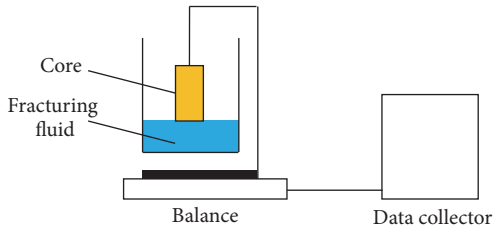

FIGURE 8: Schematic of spontaneous imbibition experiment (cocurrent imbibition).

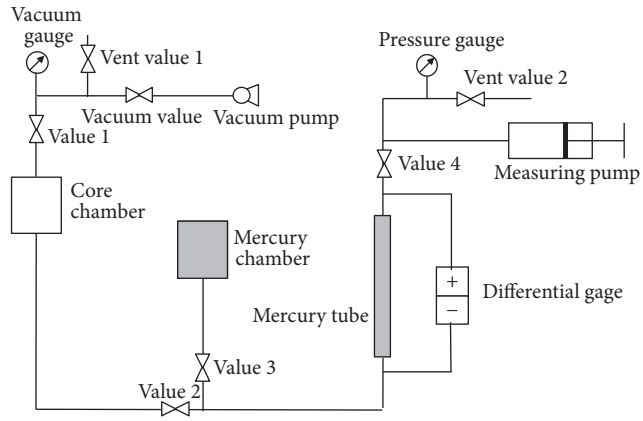

FIGURE 9: Schematic of the mercury intrusion experiment.

±5%. Place a calibration sample on imbibition experiment and note the evaporation rate for liquid. The calibration sample is a glass cylinder, with diameter 25 mm. (b) All samples are dried at temperature 338 K for 12 h before the experiment until the mass remained unchanged. Note the mass of dried samples. (c) Place the samples on imbibition experiment. When the sample contacts liquid at surface, start to record timer and data collector. (d) Correct sample's imbibition curve by calibration sample's data to eliminate the influence of liquid evaporation.

In mercury intrusion experiment, we can derive the pore size distribution of samples. The schematic diagram of mercury intrusion experiment is shown in Figure 9. Because mercury intrusion has irreversible negative effect on samples, the mercury intrusion should be arranged after permeability tests and imbibition tests. The procedure of experiment is as follows.

(a) All samples are dried at temperature 338 K for 12 h before the experiment until the mass remained unchanged.

(b) Place the samples in core chamber, close value 2 and vent value 1, open value 1, vacuum value, and start vacuum pump for 20 minutes.

(c) Open values 3 and 4, close vent value 2, and retreat measuring pump to absorb mercury. Then close value 4 and

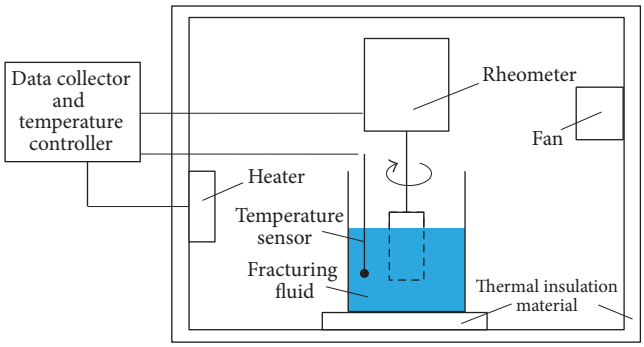

Figure 10: Schematic of viscosity instrument in this experiment.

open vent value 2 to displace air in pump. By repeating the above steps, the pump and line are filled with mercury.

(d) Keeping the environment temperature at 298 K, closing value 3 and value 1 and vent value 2, and opening values 2 and 4, the volume of injected mercury in sample increases with the increase of pumping pressure. The relationship between volume of injected mercury and pressure is recorded.

(e) When mercury cannot be injected in core sample, the retreating curve can be recorded by retreating measuring pump and recording the relationship between volume of injected mercury and pressure.

The schematic of viscosity instrument is shown in Figure 10. The measuring range for the rheometer is 1~200 mPa·s, with ±5% accuracy. The two typical fracturing fluid were prepared. This experiment can test the viscosity-temperature curve of liquid.

Conflicts of Interest

The authors declared no potential conflicts of interest with respect to the research, authorship, and/or publication of this article.

Acknowledgments

This study was supported by the National Natural Science Foundation of China (41572141).

References

[1] T. T. Palisch, M. C. Vincent, and R. J. Handren, "Slickwater fracturing: Food for thought," *SPE Production and Operations*, vol. 25, no. 3, pp. 327–344, 2010.

[2] S. A. Holditch, "Tight Gas Sands," *Journal of Petroleum Technology*, vol. 58, no. 06, pp. 86–93, 2006.

[3] J. Cai, B. Yu, M. Zou, and L. Luo, "Fractal characterization of spontaneous co-current imbibition in porous media," *Energy & Fuels*, vol. 24, no. 3, pp. 1860–1867, 2010.

[4] J. C. Cai and B. M. Yu, "A discussion of the effect of tortuosity on the capillary imbibition in porous media," *Transport in Porous Media*, vol. 89, no. 2, pp. 251–263, 2011.

[5] Y. Li, J. Yao, and Y. Yang, "The effect of the absorbed fluid layer on flow in a capillary tube," *Petroleum Science and Technology*, vol. 32, no. 2, pp. 194–201, 2014.

[6] P. Fakcharoenphol, B. Kurtoglu, H. Kazemi, S. Charoenwongsa, and Y.-S. Wu, "The effect of osmotic pressure on improve oil recovery from fractured shale formations," in *Proceedings of the SPE Unconventional Resources Conference 2014*, April 2014.

[7] C. Li, Y. Shen, H. Ge, S. Su, and Z. Yang, "Analysis of spontaneous imbibition in fractal tree-like network system," *Fractals. Complex Geometry, Patterns, and Scaling in Nature and Society*, vol. 24, no. 3, 1650035, 12 pages, 2016.

[8] C. Li, Y. Shen, H. Ge et al., "Analysis of capillary rise in asymmetric branch-like capillary," *Fractals. Complex Geometry, Patterns, and Scaling in Nature and Society*, vol. 24, no. 2, 1650024, 10 pages, 2016.

[9] Y. Shen, C. Li, H. Ge, X. Yang, and X. Zeng, "Spontaneous imbibition in asymmetric branch-like throat structures in unconventional reservoirs," *Journal of Natural Gas Science and Engineering*, vol. 44, pp. 328–337, 2017.

[10] Y. Shen, H. Ge, C. Li et al., "Water imbibition of shale and its potential influence on shale gas recovery—a comparative study of marine and continental shale formations," *Journal of Natural Gas Science and Engineering*, vol. 35, pp. 1121–1128, 2016.

[11] Y. Feng and K. E. Gray, "A parametric study for wellbore strengthening," *Journal of Natural Gas Science and Engineering*, vol. 30, pp. 350–363, 2016.

[12] Y. Feng and K. E. Gray, "A fracture-mechanics-based model for wellbore strengthening applications," *Journal of Natural Gas Science and Engineering*, vol. 29, pp. 392–400, 2016.

[13] Y. Feng, C. Arlanoglu, E. Podnos, E. Becker, and K. E. Gray, "Finite-element studies of hoop-stress enhancement for wellbore strengthening," *SPE Drilling & Completion*, vol. 30, no. 1, pp. 38–51, 2015.

[14] Y. Feng, J. F. Jones, and K. E. Gray, "A Review on fracture-initiation and -propagation pressures for lost circulation and wellbore strengthening," *SPE Drilling & Completion*, vol. 31, no. 2, pp. 134–144, 2016.

[15] P. Chen, D. Gao, Z. Wang, and W. Huang, "Study on multi-segment friction factors inversion in extended-reach well based on an enhanced PSO model," *Journal of Natural Gas Science and Engineering*, vol. 27, pp. 1780–1787, 2015.

[16] P. Chen, D. Gao, Z. Wang, and W. Huang, "Study on aggressively working casing string in extended-reach well," *Journal of Petroleum Science Engineering*, vol. 157, 2017.

[17] J. Cai, E. Perfect, C.-L. Cheng, and X. Hu, "Generalized modeling of spontaneous imbibition based on hagen-poiseuille flow in tortuous capillaries with variably shaped apertures," *Langmuir*, vol. 30, no. 18, pp. 5142–5151, 2014.

[18] Y. Shen, H. Ge, S. Su, D. Liu, Z. Yang, and J. Liu, "Imbibition characteristic of shale gas formation and water-block removal capability," *Scientia Sinica Physica, Mechanica & Astronomica*, 2017.

[19] Y. Shen, H. Ge, M. Meng, Z. Jiang, and X. Yang, "Effect of water imbibition on shale permeability and its influence on gas production," *Energy & Fuels*, vol. 31, no. 5, pp. 4973–4980, 2017.

[20] H. Dehghanpour, H. A. Zubair, A. Chhabra, and A. Ullah, "Liquid intake of organic shales," *ENERGY & FUELS*, vol. 26, no. 9, pp. 5750–5758, 2012.

[21] B. Roychaudhuri, J. Xu, T. T. Tsotsis, and K. Jessen, "Forced and Spontaneous Imbibition Experiments for Quantifying Surfactant Efficiency in Tight Shales," in *Proceedings of the SPE Conference*, 2014.

[22] F. Javadpour, "Nanopores and apparent permeability of gas flow in mudrocks (shales and siltstone)," *Journal of Canadian Petroleum Technology*, vol. 48, no. 8, pp. 16–21, 2009.

[23] C. H. Sondergeld, K. E. Newsham, J. T. Comisky, M. C. Rice, and C. S. Rai, "Petrophysical considerations in evaluating and producing shale gas resources," in *Proceedings of the SPE Unconventional Gas Conference*, Society of Petroleum Engineers, Pittsburgh, Pa, USA, 2010.

[24] F. Javadpour, M. McClure, and M. E. Naraghi, "Slip-corrected liquid permeability and its effect on hydraulic fracturing and fluid loss in shale," *Fuel*, vol. 160, pp. 549–559, 2015.

[25] A. Afsharpoor and F. Javadpour, "Liquid slip flow in a network of shale noncircular nanopores," *Fuel*, vol. 180, pp. 580–590, 2016.

[26] Z. Zhou, X. Cui, and W. Zhang, "The relationship between formation temperature and permeability in a heavy oil reservoir," *Petroleum Science and Technology*, vol. 34, pp. 31–36, 2016.

[27] B. M. Yu and P. Cheng, "A fractal permeability model for bi-dispersed porous media," *International Journal of Heat and Mass Transfer*, vol. 45, no. 14, pp. 2983–2993, 2002.

[28] J.-C. Cai, B.-M. Yu, M.-F. Mei, and L. Luo, "Capillary rise in a single tortuous capillary," *Chinese Physics Letters*, vol. 27, no. 5, Article ID 054701, 2010.

[29] S. Diamond and W. L. Dolch, "Generalized log-normal distribution of pore sizes in hydrated cement paste," *Journal of Colloid and Interface Science*, vol. 38, no. 1, pp. 234–244, 1972.

[30] S. I. Hwang and S. E. Powers, "Using particle-size distribution models to estimate soil hydraulic properties," *Soil Science Society of America Journal*, vol. 67, no. 4, pp. 1103–1112, 2003.

[31] J. Restolho, A. P. Serro, J. L. Mata, and B. Saramago, "Viscosity and surface tension of 1-ethanol-3-methylimidazolium tetrafluoroborate and 1-methyl-3-octylimidazolium tetrafluoroborate over a wide temperature range," *Journal of Chemical & Engineering Data*, vol. 54, no. 3, pp. 950–955, 2013.

[32] M. Zheng, J. Tian, and Á. Mulero, "New correlations between viscosity and surface tension for saturated normal fluids," *Fluid Phase Equilibria*, vol. 360, pp. 298–304, 2013.

[33] R. B. Haj-Kacem, N. Ouerfelli, J. Herráez, M. Guettari, H. Hamda, and M. Dallel, "Contribution to modeling the viscosity Arrhenius-type equation for some solvents by statistical correlations analysis," *Fluid Phase Equilibria*, vol. 383, pp. 11–20, 2014.

[34] D. S. Viswanath, T. K. Ghosh, D. H. L. Prasad, N. V. K. Dutt, and K. Y. Rani, "Viscosity of liquids," *AIChE Journal*, vol. 2, no. 3, pp. 290–295, 2007.

[35] D. Das, A. Messaâdi, N. Dhouibi, N. Ouerfelli, and A. H. Hamzaoui, "Viscosity Arrhenius activation energy and derived partial molar properties in N,N-Dimethylacetamide + water binary mixtures at temperatures from 298.15 to 318.15 K," *Physics and Chemistry of Liquids*, vol. 51, no. 5, pp. 677–685, 2013.

[36] H. Salhi, M. Dallel, Z. Trabelsi, N. O. Alzamel, M. A. Alkhaldi, and N. Ouerfelli, "Viscosity arrhenius activation energy and derived partial molar properties in methanol + n, n-dimethylacetamide binary mixtures the temperatures from 298.15 k to 318.15 k," *Physics Chemistry of Liquids*, vol. 51, pp. 677–685, 2013.

[37] M. Dallel, D. Das, E. S. Bel Hadj Hmida, N. A. Al-Omair, A. A. Al-Arfaj, and N. Ouerfelli, "Derived partial molar properties investigations of viscosity Arrhenius parameters in formamide + N,N-dimethylacetamide systems at different temperatures," *Physics and Chemistry of Liquids*, vol. 52, no. 3, pp. 442–451, 2014.